Mine Water and the Environment (2025) 44:78–92
https://doi.org/10.1007/s10230-025-01022-7

TECHNICAL ARTICLE

The Mechanisms Controlling the Characteristics of Groundwater in the Qinan Coal Mine

Xinyue Cai[1] · Luwang Chen[1] · Xiaowei Hou[1] · Miao Zhang[1] · Yongsheng Hu[1] · Qinghua Ou[1] · Jiawei Song[1] · Minghui Wu[1] · Xiaoping Shi[1] · Xiaoxi Yin[1]

Received: 9 July 2024 / Accepted: 3 January 2025 / Published online: 22 January 2025

Abstract
Hierarchical cluster analysis, principal component analysis, hydrochemical illustration, and objective weighting were used to study the hydrochemical characteristics and types of water–rock interaction of the groundwater in a typical North China Coalfield mine. The geological conditions and the mining disturbance were quantitatively evaluated, and mechanisms by which they affected hydrochemical evolution were elucidated. The results show that there are three types of groundwater in the coal measures: one with high Ca^{2+}, Mg^{2+}, and SO_4^{2-}, which is oxidized disturbed water; another featuring high Na^+ and HCO_3^-, which is reduced disturbed water; and one with low ionic content, making it undisturbed water. The coefficients of geological complexity and mining disturbance intensity exhibited spatial variability, with maximum values of 0.46 and 0.8, respectively. Less oxidation of pyrite and less dissolution of carbonate and sulphate was correlated with increased geological complexity, while enhanced cation exchange and sulphate reduction correlated with decreased geological complexity.

Keywords Hydrochemical characteristics · Water–rock interaction · Quantitative evaluation · Control mechanisms · North China Coalfield

Introduction

Long-term mining inevitably disrupts the structure of aquifers and alters the dynamic conditions and hydraulic connections of groundwater, thus affecting its hydrochemical characteristics (Li et al. 2018a; Qu et al. 2021b; Zhang et al. 2022c). The formation and evolution of groundwater's hydrochemistry are not merely contingent on human activities but are also intimately linked to geological conditions (Dong et al. 2022; Sahoo and Khaoash 2020; Xia et al. 2022), which influences the enrichment and migration of chemical constituents.

Previous investigations have demonstrated that hydrochemical compositions can vary in different geological conditions (Chen et al. 2022b; Lawal et al. 2023; Li et al. 2018b). The North China Coalfield is distinguished by complex geological conditions resulting from the overlay of multi-episodic tectonic activities, which further complicate the hydrochemical characteristics (Han et al. 2013; Ju et al. 2022; Zhao and Xue 2022). Consequently, a comprehensive understanding of the hydrochemical evolution of the principal aquifers in the North China Coalfield, relative to the influence of geological conditions and mining, is useful for mining safety and groundwater resources protection.

Scholars have employed methodologies such as multivariate statistical analysis (Sun and Gui 2012; Zhang et al. 2022b), self-organizing maps (SOM) (Qu et al. 2021a), isotopic geochemistry (Huang et al. 2021; Liu et al. 2017; Qu et al. 2018), and hydrogeochemical simulation (Ju et al. 2022; Liu et al. 2017) to conduct systematic studies on the evolution of the hydrochemical field. These studies have concentrated on aspects such as groundwater seepage, aquifer conditions, and hydrogeochemical environment in coalfields. Important advancements have been made, but research concerning the mechanisms has predominantly focused on qualitatively analysing the effects of geological conditions or mining on the characteristics and evolutionary patterns of the hydrochemistry (Anggara et al. 2024; Chen and Gui 2016; Wang et al. 2023; Xu et al. 2018). There exists a scarcity of systematic studies employing quantitative analysis to assess the complexity of geological conditions

✉ Luwang Chen
luwangchen8888@163.com

[1] School of Resources and Environmental Engineering, Hefei University of Technology, Hefei 230009, China

and the intensity of mining disturbance. This gap impedes the precise delineation of the developmental trends and the intrinsic properties of the hydrochemical environment and further complicates elucidating the mechanisms governing the hydrochemical evolution of aquifers. As a result, there is a considerable uncertainty associated with water hazard prevention, water resource utilization, and groundwater protection.

The groundwater in the Permian coal measures fractured sandstone aquifers (hereinafter referred to as "coal measures groundwater") serves as a direct source of water replenishment for mines in the Huaibei coalfield. Extensive mining has altered the chemistry of the coal measures groundwater (Guo et al. 2022). In this context, we studied the Qinan Coal Mine, a relatively deep coalfield in North China. The chemical characteristics, the types of water–rock interaction, and the spatial evolutionary patterns of the coal measures groundwater were revealed by employing hierarchical cluster analysis, principal component analysis, and the hydrochemical graphical method. The geological conditions and mining disturbance were quantified utilizing mesh generation and objective weighting while a graphical method was used to elucidate the mechanisms by which geological conditions and mining control the hydrochemistry of the coal measures groundwater. The research outcomes hold theoretical and practical implications for the exploitation and conservation of groundwater resources in coalfields, as well as mine safety.

Study Area

The Qinan coal mine is located in the southeastern part of the Huaibei coalfield (Zhang et al. 2019). It is ≈ 23 km north of Suzhou City and ≈ 70 km south of Bengbu City. Minor folds are not well developed, but faults are quite widespread. A total of 922 faults have been identified by the analysis of drilling, well logging, and seismic data. The mine contains 10 seams of mineable or partially mineable coal, of which the 3_2, 7_2, and 10 are the main mineable seams. As illustrated in Fig. 1, the upper part of the Qinan coal mine was chosen as the focus of this study since it is where most of the mining sections are located.

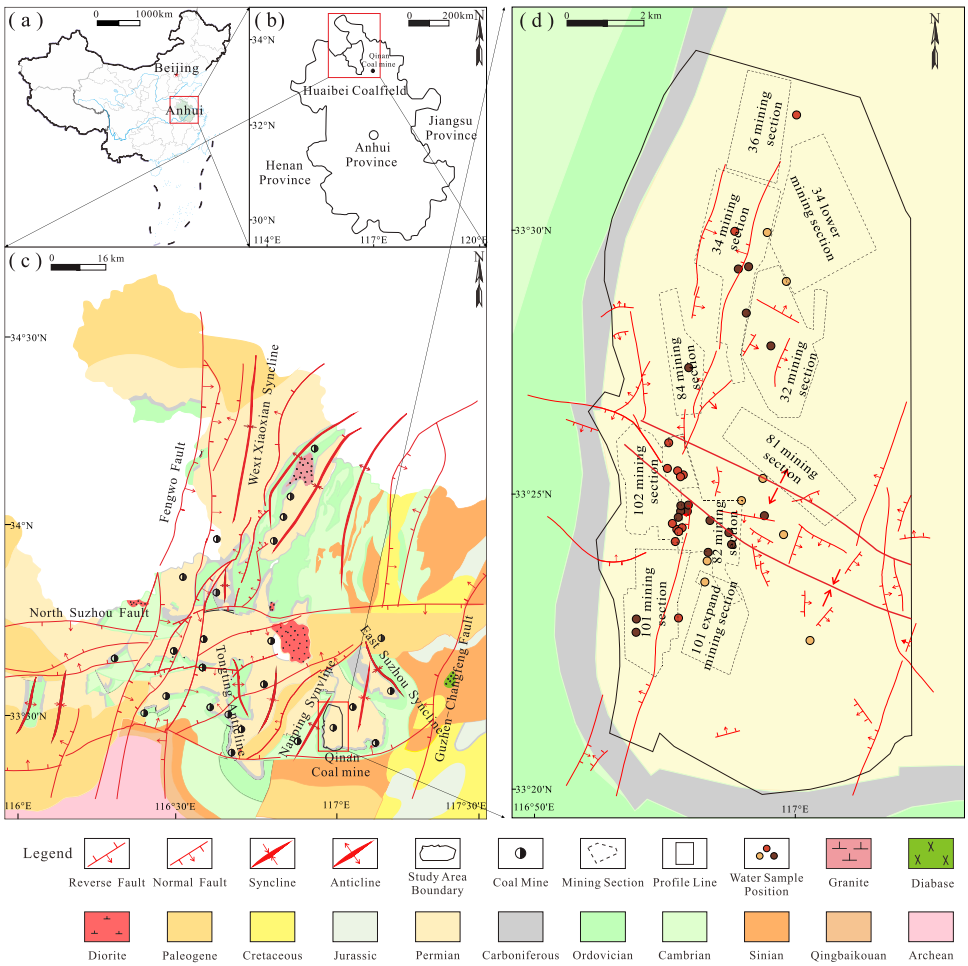

Fig. 1 Map of geological and sampling distribution of the study area

The strata in the study area, from top to bottom, are Quaternary, Neogene, Paleogene, Permian, Carboniferous, and Ordovician; the main coal-bearing strata is Permian. The representative aquifers include the loosely confined Quaternary aquifers, the fractured sandstone aquifers of the Permian coal measures, the Carboniferous Taiyuan Formation limestone aquifers, and the Ordovician limestone aquifer. Based on the lithology of the stratigraphic section and the location of the main recoverable coal seams, the Permian coal-bearing strata are divided into three aquifers and four aquicludes from top to bottom; the stratigraphic column diagram is shown in Fig. 2.

Data Collation and Analysis

Data Collation

A total of 38 sets of coal measures groundwater samples were collected at the Qinan coal mine from May 2001 to May 2022 for conventional hydrochemical analysis. The analytical data was subjected to an ion balance check using the equation:

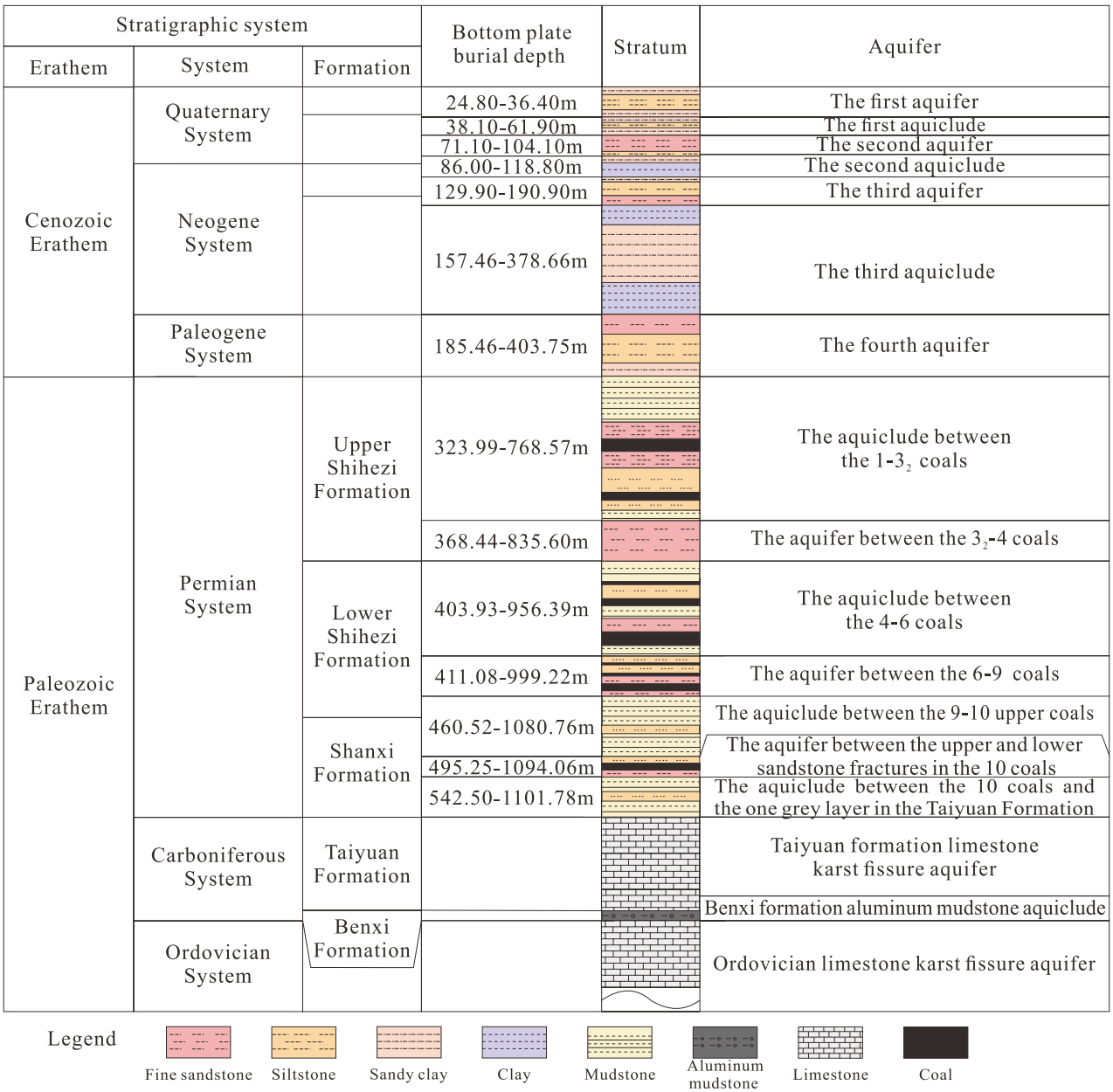

Fig. 2 Stratigraphic column diagram of the study area

$$E = \frac{\sum m_c - \sum m_a}{\sum m_c + \sum m_a} \times 100 \quad (1)$$

where E represents the relative error and m_a and m_c are the milliequivalent concentrations of anions and cations, respectively. If the E value is within the range of ± 5%, the water samples are considered acceptable. All 38 water samples met the requirements.

Analysis Methods

Hierarchical cluster analysis (HCA) has been demonstrated to be an effective approach in the analysis of mine water. The basic idea is to classify the data into different groups, where objects within the same group exhibit a high degree of similarity. The whole process is commonly visualized using a dendrogram (Yang et al. 2020). HCA was employed in this work to group similar water samples based on conventional hydrochemical data. ($Na^+ + K^+$) was replaced by Na^+ due to the low K^+ content and the similar chemical properties of Na^+ to ($Na^+ + K^+$); the other ions used were Ca^{2+}, Mg^{2+}, Cl^-, SO_4^{2-}, and HCO_3^-. The Euclidean distance and the Ward method were identified as criteria to discriminate different groups (Zhang et al. 2022a). This method is founded on the tenet of minimum information loss through the variance of squared sums for merging clusters and has been extensively applied in hydrochemical data clustering.

Principal component analysis (PCA) is a feature extraction and data compression technique that is primarily used to study how to project the originally correlated high-dimensional data sets into low-dimensional spaces with minimal information loss (Cloutier et al. 2008). In this study, the water samples were standardized using SPSS software to obtain a matrix of correlation coefficients among the ions. Subsequently, eigenvalues, eigenvectors, and the principal component (PC) contribution rate were calculated. The PC axes were also rotated using the variance-maximum rotation method, which facilitates the analysis of the specific loadings controlling the PCs and elaborates on the water–rock interaction specifically occurring in the hydrochemical data.

Criteria importance through intercriteria correlation (CRITIC) is an objective weighting method (Hou et al. 2024). It derives the information content within the data by calculating the objective weights of individual indicators. The method employs a weighting system that assigns values to indicators based on their informational content and intercorrelation. In addition to considering the influence of indicator variability on weight, the method also accounts for potential conflicts among different indicators (Krishnan et al. 2021; Xiao et al. 2023). The Pearson correlation coefficient between factors, standard deviation formula, information content, and objective weight for each factor are shown in Eqs. 2, 3, 4, and 5, respectively:

$$\rho_{xy} = \frac{\sum_{i=1}^{n}(x_i - \bar{x})(y_i - \bar{y})}{\sqrt{\sum_{i=1}^{n}(x_i - \bar{x})^2}\sqrt{\sum_{i=1}^{n}(y_i - \bar{y})^2}} \quad (2)$$

$$\sigma = \sqrt{\frac{1}{n}\sum_{i=1}^{n}(x_i - \bar{x})^2} \quad (3)$$

$$E_j = \sigma_i \sum_{i=1}^{n}\left(1 - \rho_{ij}\right) \quad (4)$$

$$W_j = E_j / \sum_{j=1}^{n} E_j \quad (5)$$

where x_i and y_i represent the numerical values of the i^{th} data of the influence factors x and y, respectively, while $\bar{x}$ and $\bar{y}$ represent the average values of x and y, respectively.

Results and Analysis

The Main Ionic Hydrochemical Characteristics

Figure 3a represents the dendrogram resulting from HCA, wherein the 38 sets of water samples are categorized into three groups at a distance of 15, sequentially named Class A, B, and C. As shown in Table 1, for Class A, the average concentration order for cations was $Na^+ > Ca^{2+} > Mg^{2+}$, whereas the average anion concentration order was $HCO_3^- > SO_4^{2-} > Cl^-$. In contrast, Class B and C exhibited an average cation concentration order of $Na^+ > Mg^{2+} > Ca^{2+}$, and an average anion concentration order of $HCO_3^- > Cl^- > SO_4^{2-}$. Compared to the other classes, Class A is distinguished by lower average concentrations of HCO_3^- and higher average concentrations of Ca^{2+}, Mg^{2+}, and SO_4^{2-}. Class B is notable for having the highest concentrations of Na^+ and HCO_3^-, but the average concentrations of Ca^{2+} and Mg^{2+} were lower than the other classes. Class C is identified by lower concentrations of all ions, with Na^+ concentration notably lower than the other two classes, and lower concentrations of Cl^- and SO_4^{2-}.

The collected water sample data were plotted on a Piper trilinear diagram using AquaChem 3.0 software. As depicted in Fig. 3b, the cations of the three groups of water samples are distributed in the D region, whereas the anions are found in regions F and G, signifying variations in the hydrochemical types. Class A is predominantly found in region 4, with hydrochemical types mainly of SO_4·HCO_3·Cl-Na and HCO_3·Cl·SO_4-Na. Class B is primarily found in region 6, with hydrochemical types predominantly of HCO_3-Na and Cl·HCO_3-Na. Class C is distributed across regions 5 and 6, with three hydrochemical types identified, among which the Cl·HCO_3-Na type is the most prevalent, followed by HCO_3-Na and Cl·HCO_3-Na·Ca·Mg types.

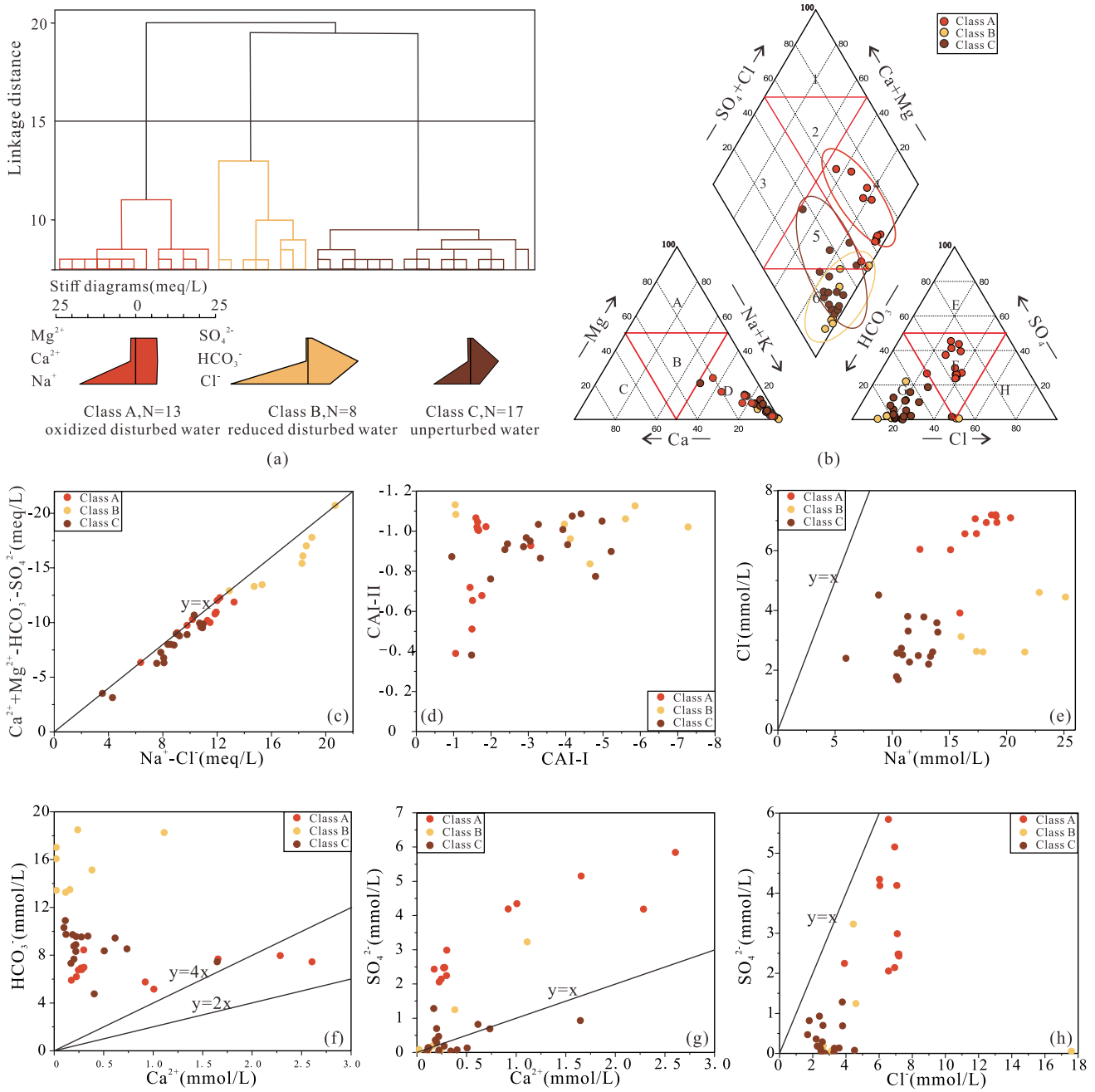

Fig. 3 **a** Dendrogram of cluster analysis for 38 coal measures groundwater. All samples are divided into 3 groups. Stiff diagrams are plotted for each group based on the mean values of hydrochemical parameters; **b** Piper trilinear diagram; **c** $Ca^{2+}+Mg^{2+}$-HCO_3^--SO_4^{2-} versus Na^+-Cl^- in meq/L; **d** CAI-II versus CAI-I in meq/L; **e** Cl^- versus Na^+ in mmol/L; **f** HCO_3^- versus Ca^{2+} in mmol/L; **g** SO_4^{2-} versus Ca^{2+} in mmol/L; **h** SO_4^{2-} versus Cl^- in mmol/L

Analysis of Water–Rock Interaction

Ion Exchange Interaction

Cation exchange refers to the exchange of cations adsorbed on the surface of soil particles and minerals by the cations present in groundwater. The presence of cation exchange in groundwater can be assessed by examining whether the value of $\rho(Ca^{2+}+Mg^{2+}$-HCO_3^--$SO_4^{2-})/\rho(Na^+$-$Cl^-)$ is close to −1 (Zhang et al. 2020). Figure 3c illustrates a notable negative correlation within the coal measures groundwater, with a slope approaching −1. This suggests the presence of cation exchange to a certain extent. The chlor-alkali indices (CAI-I and CAI-II) are frequently used to characterize the intensity

Table 1 Statistical characteristics of hydrochemical parameters (unit: meq/L)

Categories	Items	Na^+	Ca^{2+}	Mg^{2+}	Cl^-	SO_4^{2-}	HCO_3^-
Class A	Max	20.34	5.21	5.43	7.19	11.69	8.44
	Min	12.41	0.35	0.26	3.91	4.12	5.16
	Mean	17.53	1.62	1.52	6.60	6.62	6.84
Class B	Max	36.15	2.22	1.79	17.59	6.46	18.50
	Min	16.01	0.04	0.04	2.61	0.09	13.27
	Mean	24.11	0.52	0.53	6.90	1.24	15.65
Class C	Max	13.98	3.30	2.49	4.52	2.56	10.90
	Min	5.95	0.20	0.20	1.69	0.01	4.76
	Mean	11.47	0.74	0.91	2.82	0.75	8.76

of cation exchange in groundwater (Chen et al. 2022a). The cation exchange of Ca^{2+} and Mg^{2+} in groundwater with Na^+, which is adsorbed on the surface of aquifer particles, results in a negative value for both CAI-I and CAI-II. The calculation formulas are:

$$CAI{-}I = \frac{\left[r(Cl^-) - r\left(Na^+\right)\right]}{r(Cl^-)} \tag{6}$$

$$CAI{-}II = \frac{\left[r(Cl^-) - r\left(Na^+\right)\right]}{\left[r\left(SO_4^{2-}\right) + r\left(HCO_3^-\right)\right]} \tag{7}$$

where r is the ion milligram equivalent concentration.

Figure 3d illustrates that the chloro-alkali indices for all three groups of water samples were below zero, indicating that positive cation exchange was occurring between Ca^{2+} and Mg^{2+}, with varying intensities of Na^+ across the three water groups. Class B exhibits the most pronounced effect of cation exchange, as evidenced by the lower mean values of the chloro-alkali indices when compared to the other classes.

Dissolution Effect

According to Eq. 8, given the conservative behavior of Cl^- in groundwater, the ratio of $\rho(Cl^-)/\rho(Na^+)$ should be unity when the Na^+ and Cl^- are exclusively sourced from the dissolution of halite in groundwater (Liu et al. 2019). However, Fig. 3e indicates that all three groups of water samples were below the line y = x, which suggests that halite dissolution is not the sole contributor of Na^+ in the coal measures groundwater. It is therefore postulated that the excess Na^+ is derived from cation exchange processes.

Equations 9 and 10 demonstrate that in the context of groundwater, if the Ca^{2+} and HCO_3^- are a result of calcite dissolution, the ratio $\rho(HCO_3^-)/\rho(Ca^{2+})$ is expected to be 2. If these ions stem from the dissolution of dolomite, the ratio should be 4. As can be seen from Fig. 3f, Classes B and C are both situated above the line y = 4x, and most of Class A is also above this line. This distribution shows that HCO_3^- is relatively enriched compared to Ca^{2+} in the coal measures groundwater. According to Eq. 11, if SO_4^{2-} and Ca^{2+} originate exclusively from the dissolution of gypsum, the ratio $\rho(SO_4^{2-})/\rho(Ca^{2+})$ should be 1. As illustrated in Fig. 3g, a certain degree of gypsum dissolution is evident.

$$2Na^+(\text{rock}) + Ca^{2+}(\text{water}) \rightarrow 2Na^+(\text{water}) + Ca^{2+}(\text{rock}) \tag{8}$$

$$CaCO_3 + H_2O + CO_2 \rightarrow Ca^{2+} + 2HCO_3^- \tag{9}$$

$$CaMg\left(CO_3\right)_2 + 2H_2O + 2CO_2 \rightarrow Ca^{2+} + Mg^{2+} + 4HCO_3^- \tag{10}$$

$$CaSO_4 \cdot 2H_2O(\text{gypsum}) \rightarrow Ca^{2+} + SO_4^{2-} + 2H_2O \tag{11}$$

Redox Reaction

As illustrated in Fig. 3g, water samples situated above the line y = x exhibit an enrichment of SO_4^{2-} relative to Ca^{2+}, indicating alternative sources of SO_4^{2-} beyond gypsum dissolution. Mining has transformed the initially sealed geological formations into a semi-permeable oxidizing milieu, where pyrite oxidation occurs, thereby increasing the concentration of SO_4^{2-}. In addition, Class A is located above the line y = x and possesses the highest mean ratio of $\rho(SO_4^{2-})/\rho(Ca^{2+})$. Therefore, Class A represents oxidized, disturbed water. Conversely, Class C is dispersed along both sides of the y = x line and has the lowest mean ratio of $\rho(SO_4^{2-})/\rho(Ca^{2+})$, which suggests that these samples represent unperturbed water.

The ratio $\rho(SO_4^{2-})/\rho(Cl^-)$ is typically used to represent the level of sulphate reduction (Zhang et al. 2022c), as referenced in Eq. 12. The lower the ratio, the more vigorous the sulphate reduction is suggested to be. Figure 3h demonstrates that all three groups of water samples are situated below the line y = x, which indicates that there is a certain degree of sulphate reduction within the groundwater. This phenomenon is likely a result of the groundwater engaging in reductive reaction with carbonaceous materials in an

enclosed setting. Class B is observed to have a $\rho(SO_4^{2-})/\rho(Cl^-)$ ratio that is less than the other classes, which suggests that the sulphate reduction is more intense. Therefore, Class B is designated as reduced disturbed water

$$SO_4^{2-} + 2C + 2H_2O \rightarrow H_2S \uparrow + 2HCO_3^- \quad (12)$$

In conclusion, based on the ion ratio analysis, the coal measures groundwater can be categorized into three distinct types, namely, oxidized disturbed water, reduced disturbed water, and undisturbed water, corresponding to Classes A, B, and C water categories, respectively. The water–rock interaction controls the hydrochemical properties of coal measures groundwater through ion exchange, dissolution, and redox reactions. The principal types of water–rock interaction of coal measures groundwater include pyrite oxidation, dissolution of carbonate and sulphate, cation exchange, and sulphate reduction. These mechanisms interact to determine the chemical composition and characteristics of groundwater in different geological environments.

Quantification of Water–Rock Interaction

A total of 38 groundwater data samples from coal measures groundwater were standardized using the SPSS software in order to obtain a correlation coefficient matrix among the various ions. Subsequently, eigenvalues and eigenvectors were calculated to determine the contribution rates of the PCs. Selecting two PCs with eigenvalues greater than 1, the cumulative contribution rate reached 79.945%, with the first PC accounting for 45.621% of the variance and the second PC accounting for 34.324% of the variance. As shown in Fig. 4a, PC1 demonstrates high positive loadings for Ca^{2+}, Mg^{2+}, and SO_4^{2-}. This observation can be attributed to the presence of substantial amounts of carbonate and sulphate minerals within the aquifer, which undergo dissolution, as well as oxidation of pyrite, leading to elevated concentrations of these ions. PC2 is characterized by high positive loadings for Na^+, Cl^-, and HCO_3^-, with Ca^{2+} and Mg^{2+} exhibiting negative loadings. This pattern is indicative of cation exchange processes occurring as groundwater flows through the rock, where Na^+ is exchanged with the Ca^{2+} and Mg^{2+} in the water, leading to an increase in Na^+ concentration and a decrease in Ca^{2+} and Mg^{2+}. Additionally, SO_4^{2-} exhibits a negative loading, which can be ascribed to the sulphate reduction, which results in a reduction of SO_4^{2-} and a corresponding increase in HCO_3^-. PC2 is thus indicative of cation exchange and sulphate reduction.

The scores of the PC loadings for the 38 sets of water samples are plotted as a scatter diagram in Fig. 4b. In general, the three groups of water samples exhibit relatively distinct distribution characteristics. Class A has the highest mean score of the PC1 loadings (S_{PC1}), indicating that this group is predominantly influenced by dissolution of carbonate and sulphate minerals and pyrite oxidation. Mining has intensified leaching and created hydrogeochemical conditions conducive to pyrite oxidation.

The mean value for the scores of the PC2 loadings (S_{PC2}) is the highest for Class B, indicating that this class is mostly influenced by cation exchange and sulphate reduction. Given that Class B is regarded as reduced disturbed water from a chronically confined environment, cation exchange can be strengthened.

Most of the Class C water samples have a negative S_{PC1} and S_{PC2}, suggesting that relatively little water–rock interaction has occurred. This is attributed to the fact that Class C represents undisturbed water, which has been minimally affected by mining.

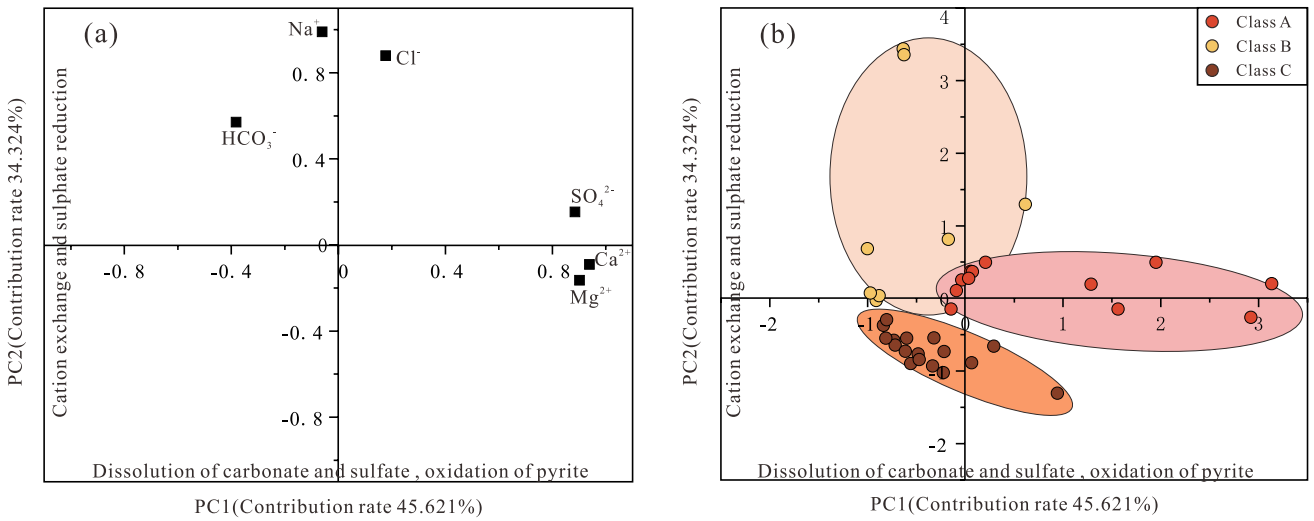

Fig. 4 Principal component analysis diagram: **a** Principal component score load diagram; **b** Scatter plot of principal component load scores

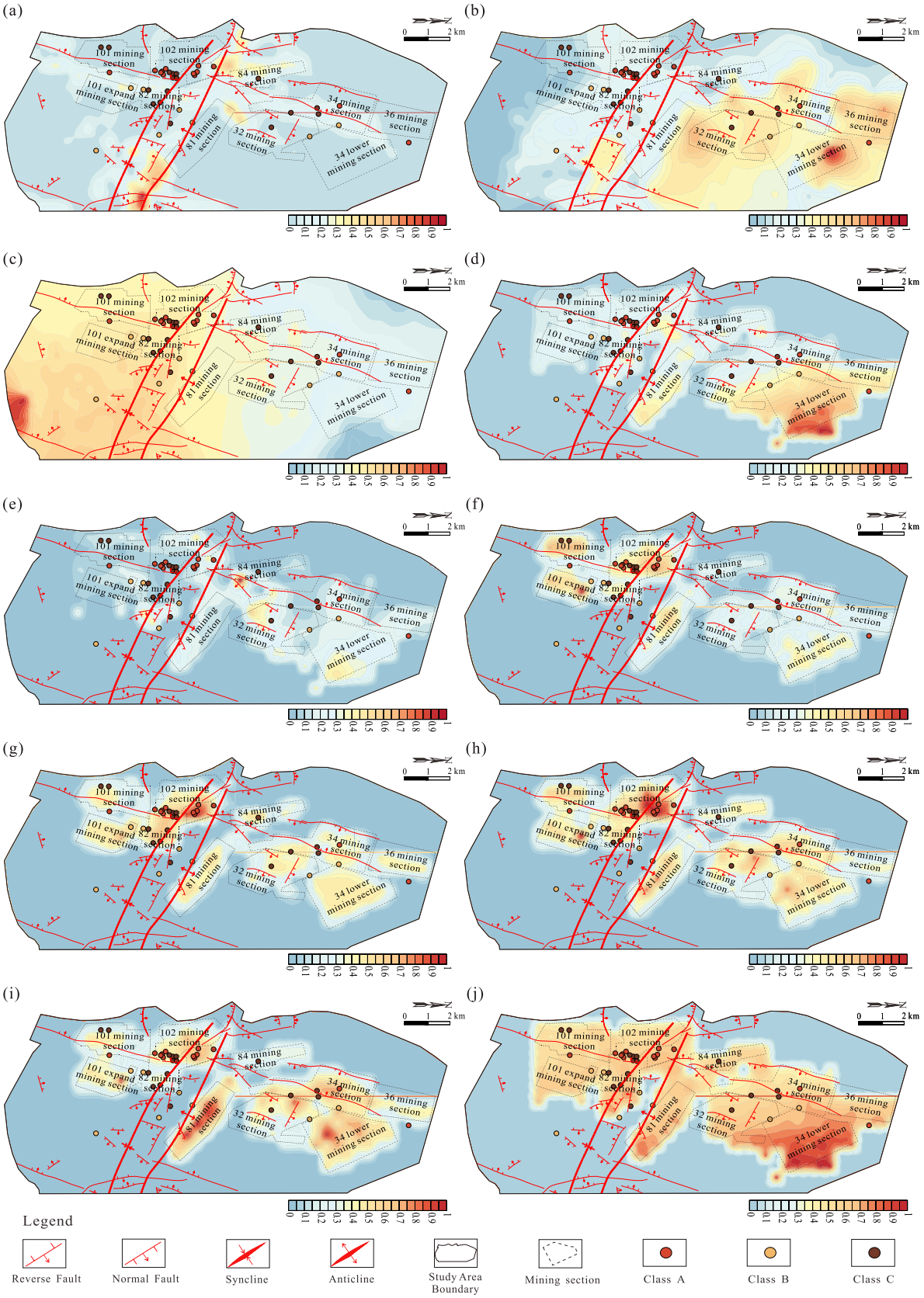
(a)
(b)
(c)
(d)
(e)
(f)
(g)
(h)
(i)
(j)
101 mining section
102 mining section
84 mining section
101 expand 82 mining section
81 mining section
32 mining section
34 mining section
34 lower mining section
36 mining section
0 1 2 km
Legend
Reverse Fault
Normal Fault
Syncline
Anticline
Study Area Boundary
Mining section
Class A
Class B
Class C

◂**Fig. 5** Quantitative results of evaluation indicators for geological conditions and mining disturbance; **a** Fault complexity coefficient; **b** Coal measures aquifer thickness; **c** Loose layer thickness; **d** Overburden thickness; **e** Mud-to-sand ratio; **f** Mining duration; **g** Mining area; **h** Mining frequency; **i** Coal mining thickness; **j** Mining depth

Quantification of Geological Conditions and Mining Disturbance

Evaluating Indicators

The study area's geological complexity was evaluated using five indicators: fault complexity coefficient, coal measures aquifer thickness, overburden thickness, loose layer thickness, and mud-to-sand ratio. These were chosen based on the information gathered from exploration lines and drilling data, as well as the geological background of the Qinan coal mine. The mining engineering plan of the study region was divided into a grid of 250 m by 250 m using a grid division concept to facilitate the analysis. Five indicators were quantified, as shown in Fig. 5.

(1) Fault complexity coefficient (G1): Faults act as conduits for groundwater, facilitating hydraulic connections between aquifers and resulting in mixing and alterations to the chemical composition of groundwater. In this study, fault complexity coefficient was calculated by the sum of the scale index of faults and the density of fault junctions and endpoints within a unit area, where the density of fault junctions and endpoints represents the total number of fault junctions and endpoints within a grid cell. From Fig. 5a, the geological structure in the eastern part of the study area is relatively simple and the fault complexity coefficient is relatively low. The maximum fault complexity coefficient is observed in the southwestern part of the study area, indicating that the fault development in this part is relatively complex and that there are multiple faults with different trends and different scales intersecting with each other.

(2) Coal measures aquifer thickness (G2): The characteristics of aquifers determine the ability of groundwater storage and migration. The Permian coal-bearing strata are divided into three aquifers from top to bottom, namely the aquifer between the 3_2–4 coals, the aquifer between the 6–9 coals, the aquifer between the upper and lower fractured sandstone in the 10 coals. Therefore, the thickness of the sandstone in the aforementioned three aquifers was taken as the coal measures aquifer thickness in the study area. From Fig. 5b, the thickness of the coal measures aquifer increases from west to east. Specifically, in the western part of the mining area, the coal measures aquifer is relatively thin. As the geographical location advances towards the east, the coal measures aquifer thickens. Concurrently, this trend also reflects the influence of differences in geological structures and sedimentary factors in the east–west direction on the thickness of the aquifer.

(3) Loose layer thickness (G3): The thickness of the loose layer is an important indicator for assessing the geological complexity as it provides valuable information on strata stability, water resources, engineering construction, and resource exploration, contributing to a more comprehensive understanding of the geological conditions in the study area. Figure 5c shows how the loose layer is relatively thin and at a relatively low level in the western portion and how it gradually thickens from west to east.

(4) Overburden thickness (G4): The thickness of the overburden is closely related to environmental factors such as groundwater resources, strata structure, and topography. The overburden thickness is the distance from the maximum working face burial depth to the basement surface. These values were statistically computed using the borehole column diagram of the study area to establish the depth of the basement surface and the burial depth of the working face. The overburden in the western region is relatively thin; the maximum overburden thickness occurs in the southeastern portion of the study area (Fig. 5d).

(5) Mud-to-sand ratio (G5): The characteristics of rock combinations exert a differential influence on the types of water–rock interaction in the groundwater, which in turn affect the chemical composition of the groundwater. The ratio of mudstone to sandstone thickness within the overburden thickness was obtained from the borehole data and indicates the distribution and composition of the overburden; the larger the ratio, the greater the proportion of mudstone. Figure 5e illustrates that the ratio in the study region is relatively low: the proportion of sandstone is relatively high in most of the study area, while the content of mudstone is comparatively low. Nevertheless, in certain specific regions, the ratio reaches high values, reaching its maximum value near mining Sect. 84, where the proportion of mudstone is high.

Based on the mining operation and borehole data, five indicators were selected to evaluate the intensity of disturbance caused by mining: mining time, mining area, mining frequency, coal thickness, and coal depth. Following the quantification of geological conditions, the study area's mining engineering plan was divided into a grid with a spacing of 250 m by 250 m to quantify the aforementioned five indicators, as shown in Fig. 5.

(1) Mining duration (C1): The time from the commencement to the cessation of mining operations for each working face was recorded in months. The total mining duration for each grid was obtained by aggregating the operational months of the working faces. As illustrated in Fig. 5f, the mining duration was considerably longer in the western region than in the east. Mining commenced relatively early in the west and continued for a considerable length of time. In contrast, mining in the eastern region was relatively delayed, and was relatively short. This discrepancy between the eastern and western regions has had a considerable effect on the geological environment and the hydrochemical characteristics of groundwater across the entire mine.

(2) Mined area (C2): The area of each working face within a grid was calculated. The cumulative area of all of the working faces within a grid represents the quantified mined area. From Fig. 5g, the mined area is greater in the western region than in the eastern region. The mining area reaches its maximum value in mining Sect. 102, where a large quantity of coal has been extracted.

(3) Mining frequency (C3): The number of working faces within each grid was counted. The sum of these counts across all grids provides the quantified value for mining frequency. From Fig. 5h, it is obvious that the study region has been affected by repeated mining to different degrees and presents diverse manifestations in different areas. The mining frequency reached its maximum value in mining Sect. 102.

(4) Mining thickness (C4): The thickness of each working face in the grid was counted and added up, thus providing a quantitative value of total mined coal thickness. As illustrated in Fig. 5i, the mined thickness peaked in mining Sect. 81. The mining operations in this area were relatively thick, thereby providing a relatively abundant reserve foundation for the mining. In contrast, the mining thickness was least in Sect. 84, which may be due to the difference in geological structure, creating a sharp contrast with Sect. 81 in terms of mining output and mining efficiency.

(5) Mining depth (C5): The maximum coal mining depth within each grid was identified and recorded. From Fig. 5j, overall, the mining depth in the study region was relatively deep and the spatial differences between each mining section are not noteworthy. This means that in most of the study area, the level of mining depth was relatively close, without meaningful depth differences or extreme depth changes. Among the mining sections, Sect. 34 had the greatest mining depth.

Quantitative Results

In this study, data from 282 boreholes within the study area was collected, and the values for the aforementioned geological indicators were statistically analysed. After normalizing the grid data for each indicator, the weights for each evaluative indicator were calculated using the CRITIC method. Table 2 shows that the thickness of the loose layer was given the highest weight, while the mud-to-sand ratio was given the lowest weight. This indicates that the thickness of the loose layer has the greatest influence on the complexity of the geological conditions within the study area, while the mud-to-sand ratio has a minor influence. The quantification results of the geological conditions were weighted by the normalized grid data of each indicator. The contour map of the results was facilitated using Surfer software and is depicted in Fig. 6a, which shows that the coefficient of geological complexity displays spatial differences. Overall, the eastern part of the study area is higher than the western part of the trend, and the geological conditions in the western region are relatively simple and stable. Due to the comprehensive influence of various geological factors, there are many complex geological phenomena in the eastern region. The maximum complexity value appeared in a low mining section, 34, in the northeast of the study area, with a value of 0.46. This is due to the greater thickness of the aquifer and overburden in the region.

Furthermore, mining information was systematically collected for a total of 72 working faces from 10 mining sections in the study area to statistically determine the value of each of the above indicators. Similar to the quantification

Table 2 Calculation results of weights for quantitative evaluation indicators of geological conditions

Indicators	Correlation coefficient					Standard deviation	Information content	Objective weight
	G1	G2	G3	G4	G5			
G1	1	0.014	0.229	−0.004	0.026	0.111	0.415	0.160
G2	0.014	1	−0.249	0.388	0.3	0.172	0.610	0.235
G3	0.229	−0.249	1	−0.16	−0.079	0.160	0.679	0.262
G4	−0.004	0.388	−0.16	1	0.757	0.189	0.571	0.220
G5	0.026	0.3	−0.079	0.757	1	0.107	0.321	0.124

G1 represents fault complexity coefficient, *G2* represents coal measures aquifer thickness, *G3* represents loose layer thickness, *G4* represents overburden thickness, *G5* represents mud-to-sand ratio

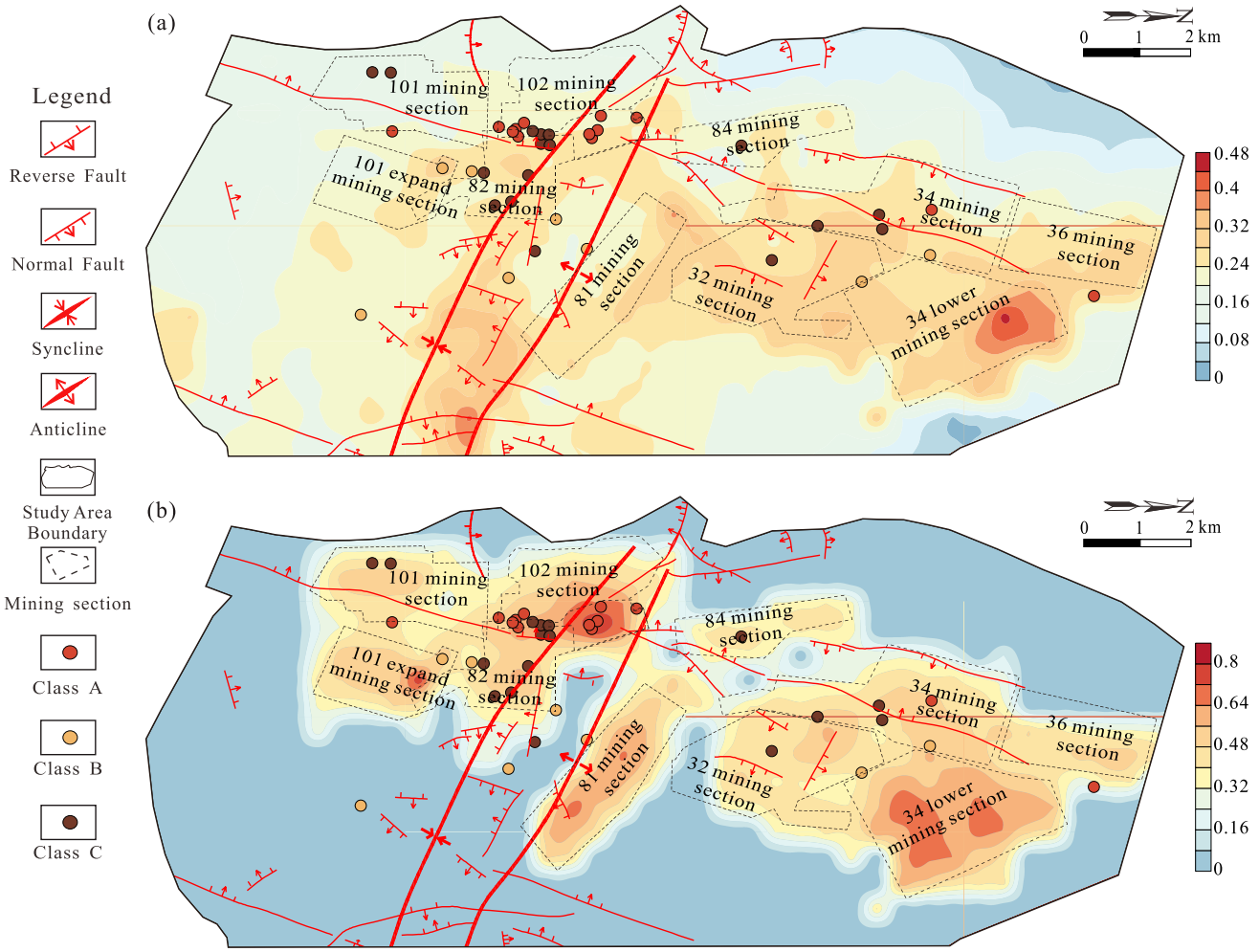

Fig. 6 Quantitative results of geological conditions and mining disturbance; **a** The coefficient of geological conditions complexity; **b** the coefficient of mining disturbance intensity

of geological conditions, the quantification results of the mining disturbance were weighted by the normalisation of the grid data of each indicator. The weights of each indicator are shown in Table 3, in which the mining duration has the largest weight and the mining depth has the smallest, indicating that the intensity of mining disturbance is mainly affected by the duration of mining. From Fig. 6b, it can be seen how different mining sections were affected by mining disturbance. The maximum value of the coefficient of mining disturbance intensity (0.8) appears in the intersection area of mining Sects. 82 and 102. This is due to the long mining duration, large mining area, and frequent mining in this area. Mining Sect. 34 has the largest area of mining disturbance, with the coefficient ranging from 0.32 to 0.72.

Table 3 Calculation results of weights for quantitative evaluation indicators of mining disturbance

Indicators	Correlation coefficient					Standard deviation	Information content	Objective weight
	C1	C2	C3	C4	C5			
C1	1	0.728	0.776	0.783	0.742	0.307	0.298	0.427
C2	0.728	1	0.901	0.855	0.871	0.180	0.116	0.166
C3	0.776	0.901	1	0.959	0.933	0.204	0.088	0.126
C4	0.783	0.855	0.959	1	0.894	0.214	0.109	0.156
C5	0.742	0.871	0.933	0.894	1	0.156	0.088	0.125

C1 represents mining duration, *C2* represents mining area, *C3* represents mining frequency, *C4* represents coal mining thickness, *C5* represents mining depth

The five mining indicators in this area have relatively high values, especially mining depth, which is the most dominant. Nevertheless, the low values of the five mining indicators result in a relatively low coefficient of mining disturbance intensity in mining Sects. 84 and 32.

Mechanisms Controlling the Spatial Evolution of Hydrochemistry

To elucidate the mechanisms of how geological conditions and mining disturbance control the spatial evolution of coal measures groundwater hydrochemistry, the coefficient of geological complexity-PC loading score relationship map and the coefficient of mining disturbance intensity-PC loading score relationship map were plotted respectively as Figs. 7a and 7b. S_{PC1} shows a high west and a low east, suggesting a gradual weakening of carbonate and sulphate dissolution and oxidation of pyrite from west to east. The coefficient of geological complexity in the study area is low in the west and high in the east, indicating that the more complex the geological conditions, the weaker the carbonate and sulphate dissolution and the oxidation of pyrite. This can be attributed to the fact that in regions characterized by intricate geological conditions, the presence of thicker overburden rock formations can exert considerable pressure on the underlying strata. This pressure can alter the porosity and permeability of the rocks, which in turn can impede the flow of groundwater. Decreased water mobility can diminish the likelihood of contact between water and carbonate, sulphate minerals, and pyrite, thereby inhibiting dissolution and oxidation reactions. In the case of the coal measures aquifer, thicker loose layers will increase the overlying pressure, decreasing the permeability of the coal measures aquifer. This, in turn, can affect the contact area between the coal measures groundwater and the surrounding rocks, as well as the strength of the water–rock interaction. In addition, the flow of groundwater is relatively slow in thicker aquifers, which facilitates the formation of a reducing environment.

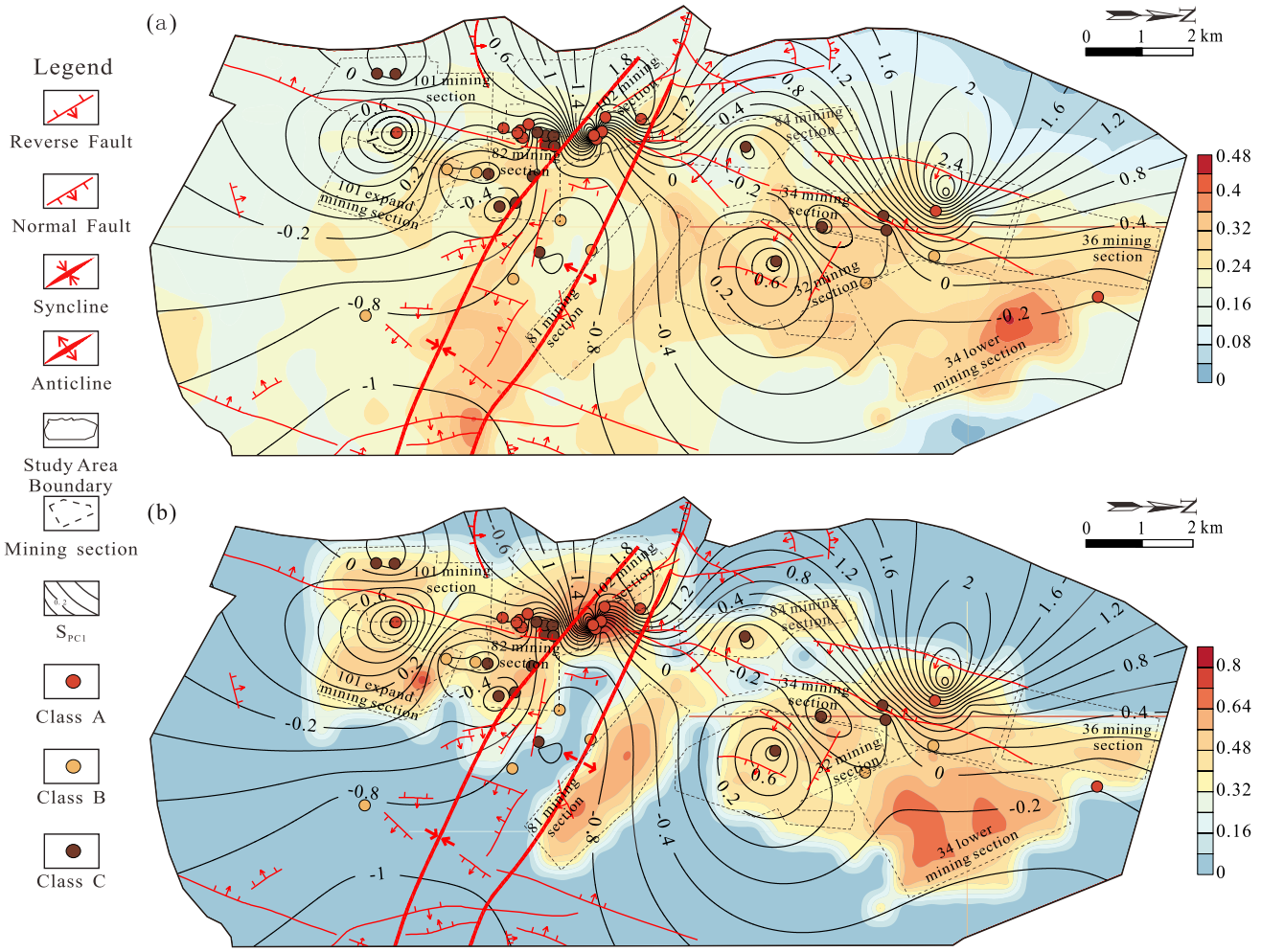

Fig. 7 The relationship between the S_{PC1} and the coefficient of geological conditions complexity and the coefficient of mining disturbance intensity: **a** S_{PC1}–the coefficient of geological conditions complexity; **b** S_{PC1}–the coefficient of mining disturbance intensity

The dissolution of carbonate and pyrite oxidation is typically impeded in a reducing environment.

Overall, regions with low coefficients of mining disturbance intensity have low S_{PC1}, and regions with high values have high S_{PC1}, so that mining contributes to the dissolution of carbonates and sulphate and the oxidation of pyrite. This is due to the fact that mining has the potential to induce fissures, subsidence and other forms of structural damage within the geological strata, and these situations will subsequently change the flow direction and velocity of groundwater, thereby increasing the possibility of water coming into contact with carbonate and sulphate minerals. In addition, the fragmentation of rocks caused by mining exposes the pyrite that was originally buried, which in turn accelerates the rate of oxidation reactions. The northwest section of the study area is less disturbed by mining, but the S_{PC1} is relatively high. The coefficient of mining disturbance intensity in mining Sect. 34 is relatively high and the S_{PC1} is relatively low because these sections are predominantly controlled by geological conditions. Specifically, the coefficient of geological complexity is lower in the northwest portion of the study area and greater in mining Sect. 34.

From Figs. 8a and 8b, it can be seen that the S_{PC2} is low in the west and high in the east, indicating that cation exchange and sulphate reduction are relatively weak in the west and relatively strong in the east. The coefficient of geological complexity is less in the west and greater in the east, which leads to the conclusion that more complex geological conditions leads to more cation exchange and less sulphate reduction. When groundwater flows through complex geological structures and contacts a variety of rocks and minerals, this can promote cation exchange reactions. At this site, mudstone accounts for a large proportion of the rock in the more complex geological areas, and clay minerals have a high cation exchange capacity because their layered structure can adsorb and release cations. Furthermore, the slow flow of groundwater allows sufficient time for interaction between groundwater and rocks, which is conducive

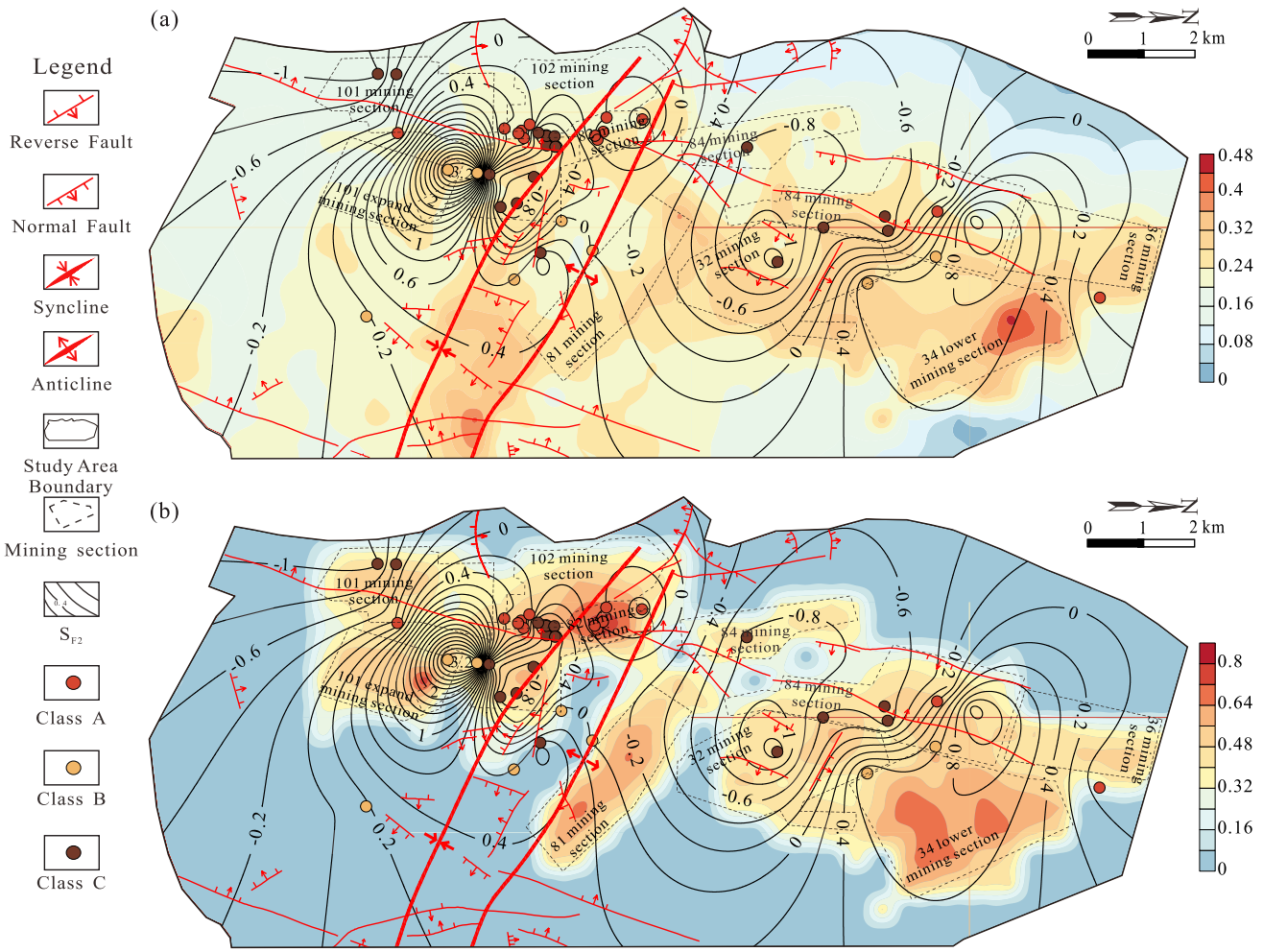

Fig. 8 The relationship between the S_{PC2} and the coefficient of geological conditions complexity and the coefficient of mining disturbance intensity: **a** S_{PC2}–the coefficient of geological conditions complexity; **b** S_{PC2}–the coefficient of mining disturbance intensity

to sulphate reduction. The presence of complex geological regions can create local hypoxic environments, which in turn provide favourable conditions for the growth and metabolic processes of sulphate-reducing bacteria. The coefficient of geological complexity in mining Sect. 32 is relatively high, and the S_{PC2} is relatively low, presumably due to strong mining disturbance.

Overall, the S_{PC2} values are relatively low in areas with high coefficients of mining disturbance intensity, and comparatively high in areas with low coefficient values, so mining has had an inverse inhibitory effect on cation exchange and sulphate reduction. Presumably, the mining damaged the originally intact rock structure, blocking or compacting the pores and cracks, greatly reducing the available sites for cation exchange. In areas with strong mining disturbance, the flow velocity of the groundwater increased, which reduces the time for cations to come into contact with rocks, making it difficult to fully carry out cation exchange reactions. Mining Sect. 34 is more affected by mining, but the S_{PC2} is relatively high, which is due to the high coefficient of geological complexity in this area, making the disturbance of mining on the groundwater chemical environment relatively small. The northwest of the study area is less disturbed by mining and is mainly controlled by geological conditions, so S_{PC2} has a lesser value.

Conclusion

There are three types of groundwater in the study area: oxidised disturbed water (Class A), reduced disturbed water (Class B), and undisturbed water (Class C). Class A is characterised by high Ca^{2+}, Mg^{2+}, and SO_4^{2-}, with the hydrochemical types primarily being SO_4·HCO_3·Cl-Na and HCO_3·Cl·SO_4-Na. Class B is characterised by high Na^+ and HCO_3^-, mainly featuring HCO_3-Na and Cl·HCO_3-Na types. Class C has low content of each ion, with hydrochemical types including Cl·HCO_3-Na, HCO_3-Na, and Cl·HCO_3-Na·Ca·Mg.

The types of water–rock interaction in the coal measures aquifer mainly include dissolution of carbonate and sulphate, oxidation of pyrite, cation exchange, and sulphate reduction. The dissolution of carbonate and sulphate and the oxidation of pyrite gradually weaken from west to east, while cation exchange and sulphate reduction are relatively weaker in the west and stronger in the east.

Of the factors assessed, loose layer thickness was the most influential aspect associated with the geological complexity. Concurrently, mining duration was the dominant factor influencing the intensity of disturbance caused by mining. The coefficient of geological complexity and the coefficient of mining disturbance intensity were spatially variable, with maximum values of 0.46 and 0.8, respectively. The coefficient of geological complexity is low in the west and high in the east, and the coefficient of mining disturbance intensity is very different in the mined section.

At this site, the more complex the geological conditions, the weaker the dissolution of carbonate and sulphate and the oxidation of pyrite, and the stronger the cation exchange and sulphate reduction. Correspondingly, mining promoted the dissolution of carbonate and sulphate and oxidation of pyrite and inhibited cation exchange and sulphate reduction.

This study has certain limitations. The geological conditions, mining methods, and hydrochemical characteristics of different coal mines vary considerably. Consequently, when applying this study to other regions, it is essential to select evaluation indicators that are tailored to the specific geological and mining conditions of the site. Furthermore, the hydrochemical characteristics of coal mines are influenced not only by the effects of mining and the geological conditions of the region, but also by external factors such as precipitation and the recharge of surface water. It is possible that these external factors themselves may be subject to uncertainty, which could result in certain objective differences in the research results.

Acknowledgements This work was financially supported by the National Natural Science Foundation of China (grant 41972256). The authors also thank the reviewers for their careful reading and valuable comments that helped improved the quality of our paper.

Data availability The datasets used during the current study are available from the corresponding author on reasonable request.

References

Anggara F, Patria AA, Rahmat B, Wibisono H, Putera MZJ, Petrus HTBM, Erviana F, Handini E, Amijaya DH (2024) Signature characteristics of coal geochemistry from the Eocene Tanjung Formation and the Miocene Warukin Formation, Barito Basin: insights into geological control on coal deposition and future critical element prospection. Int J Coal Geol 282:104423. https://doi.org/10.1016/j.coal.2023.104423

Chen S, Gui HR (2016) Hydrogeochemical characteristics of groundwater in the limestone aquifers of the Taiyuan Group and its geological significance in the Suxian mining area. Hydrogeol Eng Geol 43:33–41

Chen K, Liu QM, Liu Y, Peng WH, Wang ZT, Zhao X (2022a) Hydrochemical characteristics and source analysis of deep groundwater in Qianyingzi coal mine. Coal Geol Explor 50:12

Chen K, Liu QM, Peng WH, Liu XH (2022b) Source apportionment and natural background levels of major ions in shallow groundwater using multivariate statistical method: a case study in Huaibei Plain. China J Environ Manage 301:113806. https://doi.org/10.1016/j.jenvman.2021.113806

Cloutier V, Lefebvre R, Therrien R, Savard MM (2008) Multivariate statistical analysis of geochemical data as indicative of the hydrogeochemical evolution of groundwater in a sedimentary rock aquifer system. J Hydrol 353:294–313. https://doi.org/10.1016/j.jhydrol.2008.02.015

Dong FY, Yin HY, Cheng WJ, Li YJ, Qiu M, Zhang CW, Tang RQ, Xu GL, Zhang LF (2022) Study on water inrush pattern of Ordovician limestone in North China Coalfield based on hydrochemical characteristics and evolution processes: a case study in Binhu and Wangchao coal mine of Shandong Province. China J Clean Prod 380:134954. https://doi.org/10.1016/j.jclepro.2022.134954

Guo C, Gao JZ, Wang SQ, Zhang C, Li XL, Gou J, Lu LL (2022) Groundwater geochemical variation and controls in coal seams and overlying strata in the Shennan mining area, Shaanxi, China. Mine Water Environ 41:614–628. https://doi.org/10.1007/s10230-022-00867-6

Han Y, Wang GC, Cravotta CA III, Hu WY, Bian YY, Zhang ZW, Liu YY (2013) Hydrogeochemical evolution of Ordovician limestone groundwater in Yanzhou, North China. Hydrol Process 27:2247–2257. https://doi.org/10.1002/hyp.9297

Hou GL, Wang JJ, Fan YZ, Zhang JH, Huang CZ (2024) A novel wind power deterministic and interval prediction framework based on the critic weight method, improved northern goshawk optimization, and kernel density estimation. Renew Energ 226:120360. https://doi.org/10.1016/j.renene.2024.120360

Huang PH, Hu YS, Gao HF, Su QQ (2021) Dynamic identification and radium–radon response mechanism of floor mixed water source in high ground temperature coal mine. J Hydrol 603:126942. https://doi.org/10.1016/j.jhydrol.2021.126942

Ju QD, Hu YB, Liu QM, Liu Y, Hu TF (2022) Key hydrological process of a multiple aquifer flow system in the mining area of Huaibei plain, eastern China. Appl Geochem 140:105270. https://doi.org/10.1016/j.apgeochem.2022.105270

Krishnan AR, Kasim MM, Hamid R, Ghazali MF (2021) A modified CRITIC method to estimate the objective weights of decision criteria. Symmetry 13:973

Lawal A, Tijani MN, Snow D, D'Alessio M (2023) Quality and hydrochemical assessment of groundwater in geological transition zones: a case study from NE Nigeria. Environ Sci Pollut Res 30:10643–10663. https://doi.org/10.1007/s11356-022-22762-x

Li PY, Wu JH, Tian R, He S, He XD, Xue CY, Zhang K (2018a) Geochemistry, hydraulic connectivity and quality appraisal of multilayered groundwater in the Hongdunzi Coal Mine, Northwest China. Mine Water Environ 37:222–237

Li XY, Wu H, Qian H, Gao YY (2018b) Groundwater chemistry regulated by hydrochemical processes and geological structures: a case study in Tongchuan. China Water 10:338. https://doi.org/10.3390/w10030338

Liu P, Hoth N, Drebenstedt C, Sun YJ, Xu ZM (2017) Hydro-geochemical paths of multi-layer groundwater system in coal mining regions—Using multivariate statistics and geochemical modeling approaches. Sci Total Environ 601:1–14. https://doi.org/10.1016/j.scitotenv.2017.05.146

Liu P, Yang M, Sun Y (2019) Hydro-geochemical processes of the deep Ordovician groundwater in a coal mining area, Xuzhou, China. Hydrogeol J 27:2231–2244. https://doi.org/10.1007/s10040-019-01991-4

Qu S, Wang GC, Shi ZM, Xu QY, Guo YY, Ma L, Sheng YZ (2018) Using stable isotopes (δD, δ 18 O, δ 34 S and 87 Sr/86 Sr) to identify sources of water in abandoned mines in the Fengfeng coal mining district, northern China. Hydrogeol J 26:1443–1453. https://doi.org/10.1007/s10040-018-1803-5

Qu S, Shi ZM, Liang XY, Wang GC, Han JQ (2021a) Multiple factors control groundwater chemistry and quality of multi-layer groundwater system in Northwest China coalfield—Using self-organizing maps (SOM). Geochem Explor 227:106795. https://doi.org/10.1016/j.gexplo.2021.106795

Qu S, Shi ZM, Wang GC, Han JQ (2021b) Application of multiple approaches to investigate hydraulic connection in multiple aquifers system in coalfield. J Hydrol 595:125673. https://doi.org/10.1016/j.jhydrol.2020.125673

Sahoo S, Khaoash S (2020) Impact assessment of coal mining on groundwater chemistry and its quality from Brajrajnagar coal mining area using indexing models. Geochem Explor 215:106559. https://doi.org/10.1016/j.gexplo.2020.106559

Sun LH, Gui HR (2012) Establishment of water source discrimination model in coal mine by using hydrogeochemistry and statistical analysis: a case study from Renlou coal mine in northern Anhui Province, China. J Coal Sci Eng (China) 18:385–389. https://doi.org/10.1007/s12404-012-0409-0

Wang CY, Liao F, Wang GC, Qu S, Mao HR, Bai YF (2023) Hydrogeochemical evolution induced by long-term mining activities in a multi-aquifer system in the mining area. Sci Total Environ 854:158806. https://doi.org/10.1016/j.scitotenv.2022.158806

Xia QW, He JT, Li BH, He BN, Huang JX, Guo ML, Luo D (2022) Hydrochemical evolution characteristics and genesis of groundwater under long-term infiltration (2007–2018) of reclaimed water in Chaobai River. Beijing Water Res 226:119222. https://doi.org/10.1016/j.watres.2022.119222

Xiao JL, Xu ZS, Wang XX (2023) An improved MULTIMOORA with CRITIC weights based on new equivalent transformation functions of nested probabilistic linguistic term sets. Soft Comput 27:11629–11646. https://doi.org/10.1007/s00500-023-08218-5

Xu K, Dai GL, Zhao D, Xue XY (2018) Hydrogeochemical evolution of an Ordovician limestone aquifer influenced by coal mining: a case study in the Hancheng mining area, China. Mine Water Environ 37:238–248. https://doi.org/10.1007/s10230-018-0519-z

Yang J, Ye M, Tang ZH, Jiao T, Song XY, Pei YZ, Liu HH (2020) Using cluster analysis for understanding spatial and temporal patterns and controlling factors of groundwater geochemistry in a regional aquifer. J Hydrol 583:124594. https://doi.org/10.1016/j.jhydrol.2020.124594

Zhang H, Xing HF, Yao DX, Liu LL, Xue DR, Guo F (2019) The multiple logistic regression recognition model for mine water inrush source based on cluster analysis. Environ Earth Sci 78:1–15. https://doi.org/10.1007/s12665-019-8624-2

Zhang J, Chen LW, Chen YF, Ge RT, Ma L, Zhou KD, Shi XP (2020) Discrimination of water-inrush source and evolution analysis of hydrochemical environment under mining in Renlou coal mine, Anhui Province. China Environ Earth Sci 79:61. https://doi.org/10.1007/s12665-019-8803-1

Zhang HT, Xu GQ, Zhan HB, Li X, He JH (2022a) Simulation of multi-period paleotectonic stress fields and distribution prediction of natural Ordovician fractures in the Huainan coalfield, northern China. J Hydrol 612:128291. https://doi.org/10.1016/j.jhydrol.2022.128291

Zhang J, Chen LW, Hou XW, Li J, Ren XX, Lin ML, Zhang M, Wang YX, Tian Y (2022b) Effects of multi-factors on the spatiotemporal variations of deep confined groundwater in coal mining regions, north China. Sci Total Environ 823:153741. https://doi.org/10.1016/j.scitotenv.2022.153741

Zhang M, Chen LW, Yao DX, Hou XW, Zhang J, Qin H, Ren XX, Zheng X (2022c) Hydrogeochemical processes and inverse modeling for a multilayer aquifer system in the Yuaner coal mine, Huaibei Coalfield, China. Mine Water Environ 41:775–789. https://doi.org/10.1007/s10230-022-00851-0

Zhao ZG, Xue S (2022) Multiple-level tectonic control of coalbed methane occurrence in the Huaibei coalfield of Anhui Province. China Energy 15:4977. https://doi.org/10.3390/en15144977